Solid State Communications 177 (2014) 42–45

Contents lists available at ScienceDirect

Solid State Communications

journal homepage: www.elsevier.com/locate/ssc

Pressure effect and electron diffraction on the anomalous transition in ternary superconductor $Bi_2Rh_3Se_2$

C.Y. Chen [a], C.L. Chan [a], S. Mukherjee [a], C.C. Chou [a], C.M. Tseng [b,1], S.L. Hsu [b], M.-W. Chu [b], J.-Y. Lin [c], H.D. Yang [a,*]

[a] Department of Physics, National Sun Yat-Sen University, Kaohsiung 804, Taiwan
[b] Center for Condensed Matter Sciences, National Taiwan University, Taipei 10617, Taiwan
[c] Institute of Physics, National Chiao-Tung University, Hsinchu 300, Taiwan

ARTICLE INFO

Article history:
Received 12 July 2013
Received in revised form
16 September 2013
Accepted 25 September 2013
by E.V. Sampathkumaran
Available online 3 October 2013

Keywords:
A. $Bi_2Rh_3Se_2$ ternary compound
D. Structural phase-transformation
E. Effects of pressure
E. Transmission electron microscopy

ABSTRACT

The effect of external hydrostatic pressure up to 22.23 kbar on the temperature-dependent transport properties of the ternary compound $Bi_2Rh_3Se_2$ is investigated. Interestingly, the resistive anomaly at $T_s \sim 250$ K, previously proposed as a charge-density-wave (CDW) transition, is shifted to higher temperature with increasing pressure, in distinct contrast to an established knowledge for CDW. Using temperature-dependent electron-diffraction characterizations, we have unraveled that this transition is, in effect, of a structural phase-transformation nature, experiencing the symmetry reduction from a high-symmetry *C*-centered monoclinic lattice to a low-symmetry primitive one below T_s. A more elaborately determined room-temperature *C*-centered lattice was also proposed.

1. Introduction

Over the past several decades there has been considerable interest in the coexistence of superconductivity (SC) and charge-density-wave (CDW) transition in transition metal di- and tri-chalcogenides, MX_2 and MX_3 (M=transition metal, X=S, Se, Te) [1–5]. The nature of SC is to decrease material's resistivity to zero, while CDW is to increase material's resistivity becoming semiconductor or insulator. It is an interesting behavior that a significant competition between SC and CDW coexists in the same material [6,7], which can be clearly explored by tuning physical or chemical pressure. Similar situation occurs in the ternary rare-earth-transition-metal silicides $R_5T_4Si_{10}$ (R=rare-earth elements; T=Co, Ir, Rh, and Os). For instance, $Lu_5Ir_4Si_{10}$ has been known to enhance the superconducting transition temperature under applied pressure and doping at the expense of suppressing the resistive CDW anomaly [8,9]. Currently, the number of iron-based superconductors is a real surprise and has generated tremendous interest. Specially $FeSe_x$ [10–12] could provide the most appropriate site of understanding the iron-based superconductors because of its simple structure similar to the Fe–As layer. At high pressure, there is a subtle interaction between SC and spin density wave (SDW) in $FeSe_x$ [12]. On the other hand, the high resolution electron microscopy reveals that a structural transition from tetragonal to orthorhombic in $Fe_{1.01}Se$ is a driving force for superconducting phase [13]. Thus, Se deficiency might be a key factor for stabilizing the superconducting phase in $FeSe_x$. This also suggests that the SC, SDW and structure are strongly correlated in the Fe–Se systems.

Compared to $R_5T_4Si_{10}$ and $FeSe_x$, the recently discovered parkerite-type superconductors [14,15] could also represent an intriguing class of materials for tackling the intricate interactions among the SC, CDW, SDW, and/or structural transitions. Sakamoto et al. [15] have reported a superconducting transition (~0.7 K) along with CDW state at $T_s \sim 250$ K in parkerite-type $Bi_2Rh_3Se_2$. In the report, the room-temperature crystal structure has been considered as *C*-centered monoclinic (*C*12/m1, $\beta = \sim 89.153(3)^\circ$; $a = 11.414(10)$ Å, $b = 8.3709(9)$ Å, $c = 11.989(1)$ Å), and the CDW formation was proposed through observations of superlattice peaks below T_s using X-ray powder diffraction [15]. Nevertheless, the indicated transition might not direct to an unambiguous CDW onset in the current absence of detailed band-structure knowledge and more extensive structural characterizations for $Bi_2Rh_3Se_2$ [16]. In this paper, we report the pressure effect on the resistive anomaly occurred at $T_s \sim 250$ K compared to conventional CDW and systematic temperature-dependent electron diffraction [16] to investigate the possible satellite spots resulted from CDW formation below T_s and the structural transformation across T_s.

* Corresponding author. Tel.: +886 752 537 32.
E-mail address: yang@mail.nsysu.edu.tw (H.D. Yang).
[1] Present address: Institute of Physics, Academia Sinica, Taipei 11529, Taiwan.

0038-1098/$ - see front matter © 2013 Elsevier Ltd. All rights reserved.
http://dx.doi.org/10.1016/j.ssc.2013.09.025

2. Material and methods

Crystalline $Bi_2Rh_3Se_2$ was prepared with stoichiometric mixtures (Bi:Rh:Se=2:3:2) of high-purity Bi, Rh, and Se, sintered in a quartz tube isolating from air at the maximum temperature 1320 K for 6 h and then slowly cooled with the rate of 2 K/h to 1020 K. Finally, it was water quenched to room temperature. The crystal structure of the obtained product was identified by powder X-ray diffraction (XRD) measurements using both in-house (wavelength, 1.54 Å) and synchrotron radiation facilities (wavelength, 0.62 Å; National Synchrotron Radiation Research Center, Taiwan). The magnetic susceptibility was performed in Superconducting Quantum Interference Device (SQUID) (Quantum Design, MPMS XL-7). The low-temperature specific heat was measured from 0.5 to 2 K by using a ^{3}He heat-pulsed thermal relaxation calorimeter [17]. High temperature (2–300 K) specific heat measurement was done in Physical Property Measurement System (PPMS) (Model: 6000, Quantum Design). Pressure dependent electrical resistivity measurements were executed using a four-terminal probe method in PPMS with the temperature 2–340 K under the hydrostatic pressure up to ~23 kbar using the piston-cylinder self-clamped technique [18]. An inert fluid, Daphne-7373, was used as the pressure transmitting medium along with a manometer superconducting tin. The electron diffraction characterizations were performed on a transmission electron microscopy (TEM; JEOL 2000FX) operated at 200 kV and equipped with a low-temperature sample stage. The TEM specimens were prepared by firstly crashing a sintered pellet into powders and then collecting the micro-crystalline materials using a copper grid. The temperature homogeneity and accuracy upon TEM characterizations have been faithfully controlled as reported previously [16]. An illuminating area of ~280 nm in diameter was always used upon selected-area electron diffraction (SAED).

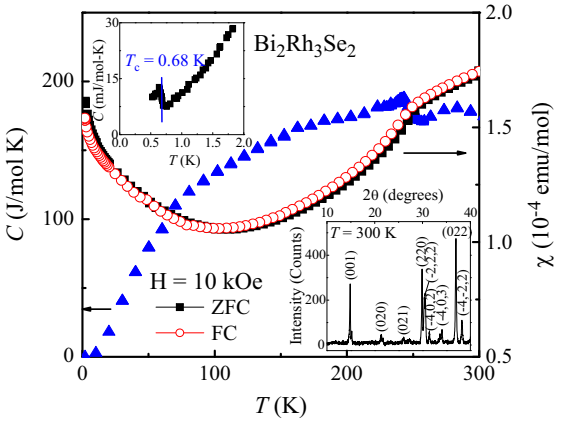

Fig. 1. (Color online) Left label: Temperature dependence of specific heat C. Right label: Temperature dependence of magnetic susceptibility χ in the presence of magnetic field 10 kOe. Lower inset: X-ray powder diffraction data at 300 K. Upper inset: C vs. T curve, where T_c=0.68 K.

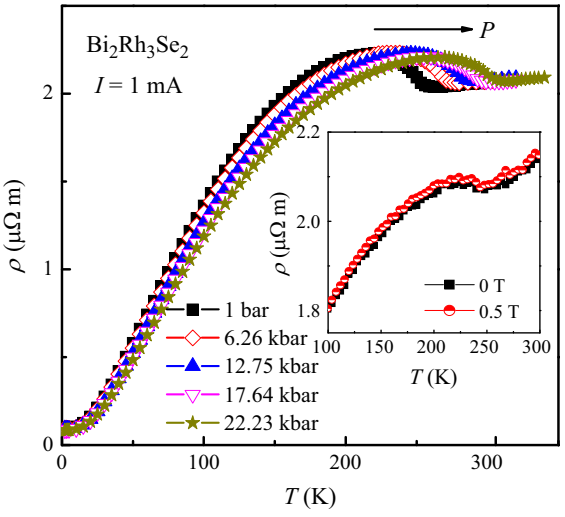

Fig. 2. (Color online) Temperature dependence of electric resistivity at different applied pressure (maximum 22.23 kbar). Inset: Temperature dependence of electric resistivity under different magnetic fields at ambient pressure.

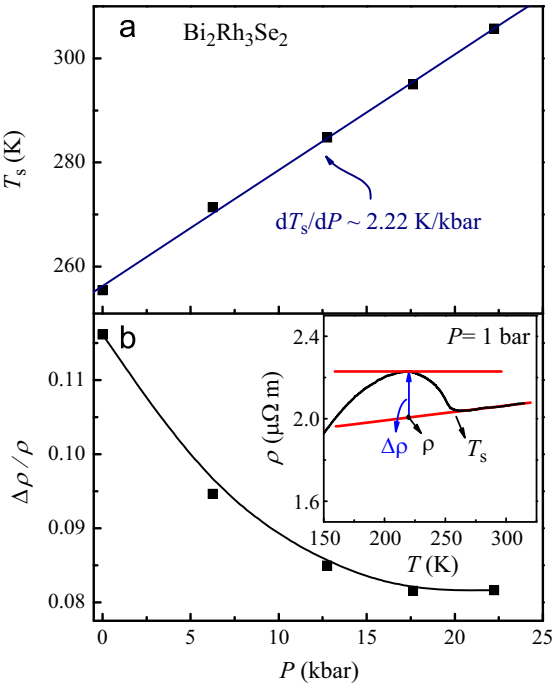

Fig. 3. (Color online) (a) Transition temperature at different pressure appears as a linear relationship, and the slope is about dT_s/dP=2.22 K/kbar. (b) The relative anomaly amplitude $\Delta\rho/\rho$ is suppressed by applied pressure. Inset: Schematic diagram of how to determine the value of $\Delta\rho$ and ρ.

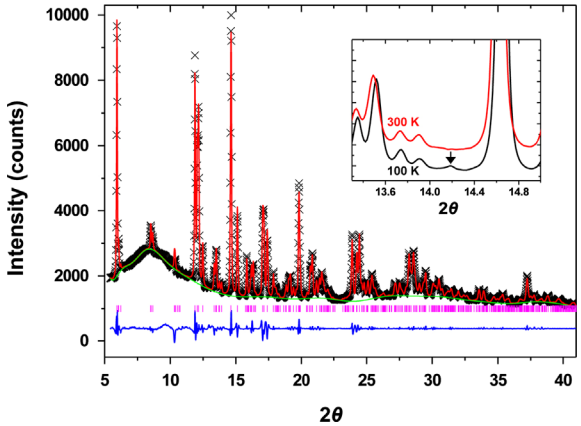

Fig. 4. (Color online) The refinement of the powder XRD pattern acquired at room temperature using synchrotron radiation source (wavelength, 0.62 Å). Red curve, the calculated powder pattern. Black crosses, the experimental data. Green curve, the background. Blue curve, the difference between the experimental and calculated intensities. Vertical bars, the Bragg reflections. Inset, blowup of the room- and low-temperature XRD patterns with the systematic appearance of addition reflections such as the one indicated by the black arrow.

3. Results and discussions

The data obtained for the temperature-dependent specific heat (C) and magnetic susceptibility (χ, after diamagnetic correction) measurements upon an applied magnetic field of 10 kOe for $Bi_2Rh_3Se_2$ are shown in Fig. 1. Below 250 K, C and χ drop gradually. In the lower and upper insets present the part of in-house, room-temperature XRD pattern and low-temperature (0.5–2 K) C–T curve, revealing a superconducting transition (T_c) at 0.68 K. The C–T measurements are in fair agreement with those in previously published report [15] and the detailed structural characterizations by synchrotron X-ray diffraction and SAED are shown later in Figs. 4 and 5.

Fig. 2 shows the temperature dependence of the resistivity between 2 and 340 K under various pressures up to 22.23 kbar. At ambient pressure a hump-like resistive anomaly is observed around $T_s \sim 250$ K, which agrees with the previous result and was previously attributed to a CDW transition [15]. However, the increasing T_s with increasing pressure in the material is inconsistent with that observed for many conventional CDW superconductors [1,6,7]. The temperature dependence of resistivity under magnetic field is also displayed in the inset of Fig. 2. No detectable shift of the resistive anomaly is observed in the presence of magnetic field, indicating that the origin for the resistive anomaly occurred at T_s is not related to SC and magnetism.

The transition temperature T_s derived from Fig. 2 under applied different pressures is illustrated in Fig. 3(a). The T_s increases linearly with P at a rate of $dT_s/dP = 2.22$ K/kbar and the relative peak intensity $\Delta\rho/\rho$ declines gradually. The increase of T_s through the application of P in $Bi_2Rh_3Se_2$ is quite intriguing. In comparison with other CDW systems, the negative pressure coefficients $dT_s/dP = -0.3$ K/kbar in 2H–$NbSe_2$ [4] and -6.25 K/kbar in $NbSe_3$ [2] have been reported. Therefore, the effective origin for the

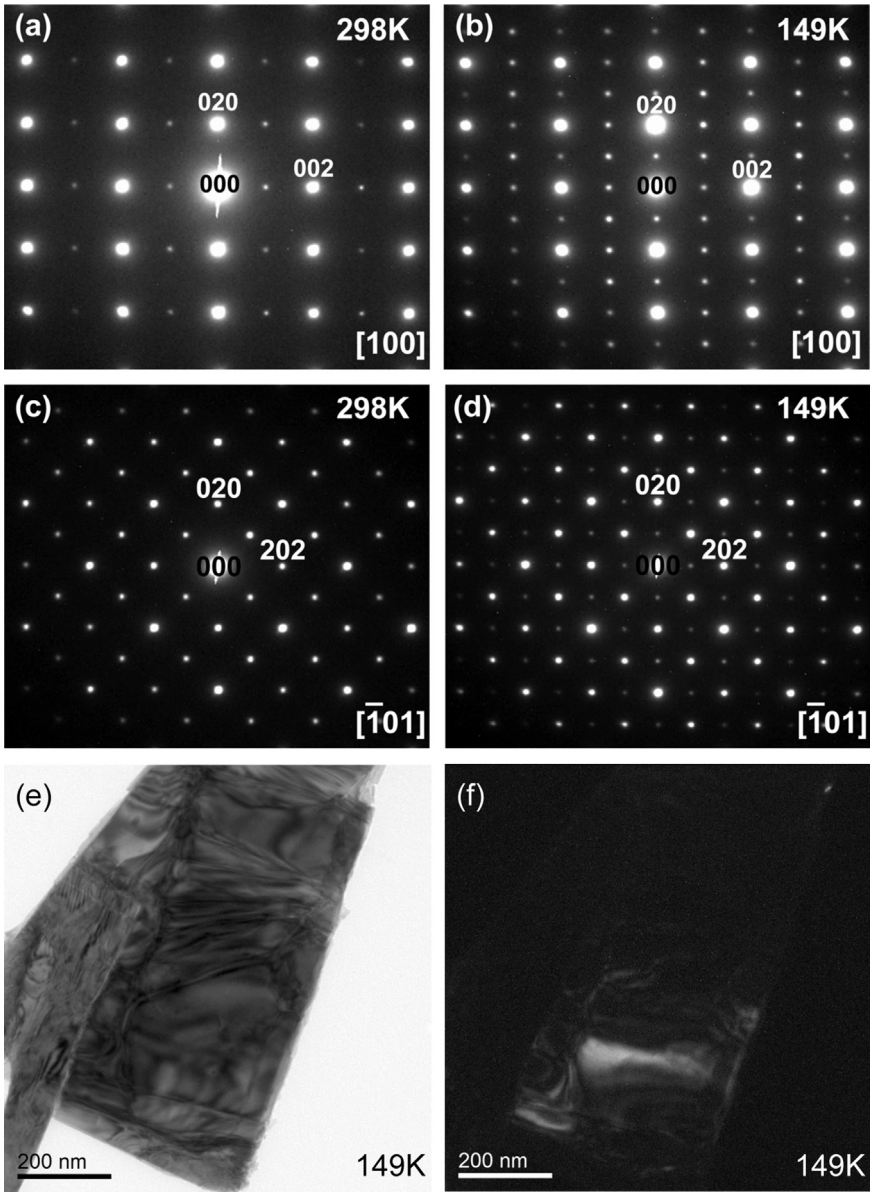

Fig. 5. SAED patterns of $Bi_2Rh_3Se_2$ obtained (a) at room temperature and (b) 149 K along [100]-projection, and at (c) room temperature and (d) 149 K along [$\bar{1}$01]-projection. All reflections observed in (a) and (c) are fully explained within the monoclinic $C12/m1$ lattice, featuring the otherwise β angle of $\sim 134^\circ$ (see text). In (b) and (d), the systematic presence of symmetry-forbidden reflections compared to (a) and (c), respectively, unravels a structural phase transition below T_s into monoclinic $P12/m1$. (e) and (f), the BF and DF images of an individual crystal taken at 149 K. The DF imaging has been acquired using $0k0$ (k=odd) type reflections and comparable diffraction contrasts were observed exploiting other symmetry-forbidden reflections.

transition upon the resistive anomaly at T_s prompts for further elaborations. We have then characterized the pressure-dependent change in resistivity ($\Delta\rho/\rho$) at the transition, as shown in Fig. 3(b). The $\Delta\rho/\rho$ decreased with pressure P is shown in Fig. 3(b) indicating the suppression of sharpness of transition with the applied pressure.

To shed more light on the resistive character in Fig. 3(b), we have performed extensive structural characterizations using XRD and SAED as shown in Figs. 4 and 5, respectively. The XRD and SAED investigations have been performed at both room and low temperatures. Moreover, the SAED patterns in Fig. 5(a)–(d) are the representative results over five thoroughly investigated single-crystalline materials with the typical bright-field (BF) image of a crystal shown in Fig. 5(e). It has been broadly recognized that an individual crystal out of the powder ensemble can be considered as a single crystal [16], which is indispensable for understanding fundamental structural characteristics. The SAED results in Fig. 5 (a)–(d) are, therefore, general characteristics, instead of specific features of given local regions.

Within the $C12/m1$ symmetry of the room-temperature structure of $Bi_2Rh_3Se_2$, it is to be pointed out that, in effect, there exist two separate unit-cell choices, the well-known one with non-orthogonal β of $\sim$89.153(3)° [15] and the other with β of $\sim$134° [19]. Our careful powder XRD refinements using either lattice choice within the pattern matching of the Rietveld method surprisingly led to similar figures of merit (both at the scale of R_{wp}, $\sim$2.4%; R_p, $\sim$1.5%; χ^2, $\sim$1.2). In Fig. 4, we show the refined result of the large-β cell with thus-obtained $a=11.413(1)$ Å, $b=8.368(2)$ Å, $c=8.336(1)$ Å, and $\beta=134.05(4)°$. Notably, the lattice volume of this unit cell is practically half of the refined small-β counterpart ($a=11.416(1)$ Å; $b=8.365(1)$ Å; $c=11.982(2)$ Å; $\beta=89.10(3)°$). Upon a given symmetry, a small-volume lattice always corresponds to an optimized periodicity of the structure [20]. To first approximations, the refined cell with $\beta\sim134°$ would represent the optimal lattice choice for $Bi_2Rh_3Se_2$, rather than the reported unit cell with $\beta\sim89°$ [15]. Our proposed lattice is indeed affirmed by the room-temperature SAED patterns shown in Fig. 5(a) and (c), the indexing of which cannot be achieved without this large-β cell.

More intriguingly, additional reflections were systematically observed below T_s in both the SAED (Fig. 5(b) and (d)) and XRD (inset, Fig. 4) investigations at 149 and 100 K, respectively. Due to the low monoclinic symmetry and large cell parameters characteristic to $Bi_2Rh_3Se_2$, non-negligible overlaps of XRD peaks take place and the additional XRD reflections can thus merge into the intensity of the pristine Bragg reflections. A further refinement of the XRD pattern at 100 K becomes tedious and the low-temperature SAED turns out to be an optimal solution for tackling the structural subtlety below the transition temperature. Indeed, a careful examination of the low-temperature SAED patterns revealed the systematic presence of reflections with $0k0$ (k=odd) and $h0l$ (h,l=odd), otherwise forbidden to $C12/m1$. Tilting the crystals away from the zone-axes did not lead to the disappearance of these symmetry-forbidden spots, indicating that they are not the product of electron multiple scattering, but real structural reflections [16]. The symmetry-breaking spots further direct to reflection conditions compatible with those of monoclinic $P12/m1$ [20]. Using these symmetry-forbidden reflections for dark-field (DF) imaging (Fig. 5(f)), only ordinary diffraction contrasts can be observed, totally free from stripe-like domains due to phase modulations in CDW phases such as those found in the DF investigations of $Ho_5Ir_4Si_{10}$ and $Lu_2Ir_3Si_5$ at low temperatures [16,21]. It can be readily suggested that T_s in $Bi_2Rh_3Se_2$ does not correspond to a CDW transition, rather a structural transition, and all our electronic characterizations in Figs. 1–3 do not seem to support the onset of a CDW transition, either. The increase of the structural transition temperature upon external pressures otherwise remains an open question.

4. Conclusions

In summary, the pressure effect up to 22.23 kbar on the electrical resistivity of $Bi_2Rh_3Se_2$ has been studied in the temperature range 2–340 K. The resistive anomaly occurred at $T_s\sim250$ K is shifted to higher temperature with increasing pressure, which is inconsistent with results observed in conventional CDW formation. The structural elaborations by XRD and SAED indicated that a structural transition from $C12/m1$ to $P12/m1$ takes place below T_s, rather than the previously suggested CDW transition.

Acknowledgment

This work was supported by the National Science Council, Taiwan under Grant no. NSC 100-2112-M-110-004-MY3.

References

[1] P. Monceau, J. Peyrard, J. Richard, P. Molinié, Physical Review Letters 39 (1977) 161.
[2] A. Briggs, P. Monceau, M. Nunez-Regueiro, J. Peyrard, M. Ribault, J. Richard, Journal of Physics C: Solid State Physics 13 (1980) 2117.
[3] K. Yamaya, M. Yoneda, S. Yasuzuka, Y. Oka-jima, S. Tanda, Journal of Physics: Condensed Matter 14 (2002) 10767.
[4] C.W. Chu, V. Diatschcnko, C.Y. Huang, F.J. DiSalvo, Physical Review B 15 (1977) 1340.
[5] D.J. Eaglesham, J.W. Steeds, J.A. Wilson, Journal of Physics C: Solid State Physics 17 (1984) L697.
[6] A.M. Gabovich, A.I. Voitenko, Low Temperature Physics 26 (2000) 305.
[7] A.M. Gabovich, A.I. Voitenko, J.F. Annett, M. Ausloos, Superconductor Science and Technology 14 (2001) R1.
[8] R.N. Shelton, L.S. Hausermann-Berg, P. Klavins, H.D. Yang, M.S. Anderson, C.A. Swenson, Physical Review B 34 (1986) 4590.
[9] H.D. Yang, P. Klavins, R.N. Shelton, Physical Review B 43 (1991) 7681.
[10] F.C. Hsu, J.Y. Luo, K.W. Yei, T.K. Chen, T.W. Huang, P.M. Wu, Y.C. Lee, Y.L. Huang, Y.Y. Chu, D.C. Yan, M.K. Wu, Proceedings of the National Academy of Sciences USA 105 (2008) 14262.
[11] W. Uhoya, G. Tsoi, Y. Vohra, N. Wolanyk, S.M. Rao, M.K. Wu, S. Weir, EPL 99 (2012) 26002.
[12] V.A. Sidorov, A.V. Tsvyashchenko, R.A. Sadykov, Journal of Physics: Condensed Matter 21 (2009) 415701.
[13] T.M. McQueen, A.J. Williams, P.W. Stephens, J. Tao, Y. Zhu, V. Ksenofontov, F. Casper, C. Felser, R.J. Cava, Physical Review Letters 103 (2009) 057002.
[14] T. Sakamoto, M. Wakeshima, Y. Hinatsu, Journal of Physics: Condensed Matter 18 (2006) 4417.
[15] T. Sakamoto, M. Wakeshima, Y. Hinatsu, K. Matsuhira, Physical Review B 75 (2007) 060503(R).
[16] C.M. Tseng, C.H. Chen, H.D. Yang, Physical Review B 77 (2008) 155131.
[17] S.J. Chen, C.F. Chang, H.L. Tsay, H.D. Yang, J.-Y. Lin, Physical Review B 58 (1998) R14753.
[18] C.L. Huang, C.C. Chou, K.F. Tseng, Y.L. Huang, F.C. Hsu, M.K. Wu, H.D. Yang, Journal of the Physical Society of Japan 78 (2009) 084710.
[19] R. Weihrich, S.F. Matar, I. Anusca, F. Pielnhofer, P. Peter, F. Bachhuber, V. Eyert, Journal of Solid State Chemistry 184 (2011) 797.
[20] T. Hahn (Ed.), International Table for Crystallography Volume A: Space-Group Symmetry, vol. 5, Springer, Berlin, 2005.
[21] M.H. Lee, C.H. Chen, M.-W. Chu, C.S. Lue, Y.K. Kuo, Physical Review B 83 (2011) 155121.